

Proton Radiation Damage and Annealing of COSI p-type Cross-strip HPGe Detectors

Sophia E. Haight^a, Steven E. Boggs^{a,b}, Gabriel Brewster^a, Sean N. Pike^a, Jarred M. Roberts^a, Albert Y. Shih^c, Joanna M. Szornel^d, John A. Tomsick^b, Aravind B. Valluvan^a, Andreas Zoglauer^b

^a*Department of Astronomy & Astrophysics, University of California, San Diego, 9500 Gilman Drive, La Jolla, CA, 92093, USA*

^b*Space Sciences Laboratory, University of California, Berkeley, 7 Gauss Way, Berkeley, CA, 94720, USA*

^c*NASA Goddard Space Flight Center, Greenbelt, MD, 20771, USA*

^d*Lawrence Berkeley National Laboratory, 1 Cyclotron Rd, Berkeley, CA, 94720, USA*

Abstract

In order to understand the effects of a space radiation environment on cross-strip germanium detectors, we investigated the effects of high-energy proton damage on a COSI detector and the capabilities of high-temperature annealing in repairing detector spectral resolution. We irradiated a COSI-balloon cross-strip high-purity germanium (HPGe) detector with a high-energy proton fluence corresponding to ~ 10 years in a space radiation environment. We repaired the resulting degradation in spectral resolution within 16% of its preradiation value through a series of high-temperature anneals. We characterize the repair of charge traps with time spent under high-temperature anneal to inform an annealing procedure for long-term maintenance of COSI's spectral resolution.

Keywords: Gamma-ray, HPGe detectors, Radiation damage, Annealing

1. Introduction

1.1. Background

The Compton Spectrometer and Imager (COSI) is a NASA Small Explorer (SMEX) satellite mission currently under development for launch in 2027 [1]. COSI is a wide-field gamma-ray telescope designed to provide spectroscopy, imaging, and polarimetry of astrophysical sources in the bandpass

0.2-5 MeV. The heart of the COSI instrument is an array of 16 cross-strip germanium detectors (GeDs) providing excellent energy resolution to achieve two of the primary mission goals. First, to uncover the origin of Galactic positrons through imaging spectroscopy of the annihilation emission at 0.511 MeV. And second, to reveal Galactic element formation through study of gamma-ray emission lines produced through radioactive decay of recently synthesized elements. To fulfill these science goals, COSI must maintain excellent spectral performance throughout its primary mission.

The spectral resolution of GeDs in space degrade due to increased charge trapping induced by radiation damage from ionizing particles, most significantly high-energy protons. High-energy protons damage the crystal lattice structure of the detectors and produce negatively ionized deformations which trap holes as they drift in the applied bias voltage towards the signal electrodes [2]. Trapping degrades spectral resolution of the hole-collection signal, characterized by the broadening of the photpeaks, as measured by the full width at half maximum (FWHM), and increased low-energy tailing of spectral lines. This degrades the ability to determine the energy of the incoming gamma-rays.

Similar radiation damage effects have been observed by germanium spectrometers INTEGRAL/SPI [3] and RHESSI [4] during their time in orbit. Both instrument teams implemented a series of high-temperature anneals at $\sim 100^\circ\text{C}$ to repair the radiation damage and restore the spectral resolution. However, annealing at these temperatures in orbit requires careful planning and design to avoid permanent damage to any instrument. The SPI telescope is composed of 19 coaxial GeDs launched into a highly eccentric orbit (perigee of 9000 km and apogee of 154600 km). After noting a significant degradation in energy resolution after 2 years in orbit, SPI began completing periodic high-temperature anneals to repair spectral resolution and prevent permanent damage from radiation [5]. SPI currently anneals at 100°C for 14 days every 6 months, observing an improvement of 10-15% to their spectral resolution between each anneal [6]. However, they suffered the loss of 2 GeDs [5]. In low earth orbit (LEO) at 38° inclination, RHESSI similarly experienced significant losses in resolution which warranted an annealing procedure. Nine segmented coaxial n-type GeDs underwent 5 anneals at 100°C over 9 years of operation, each anneal lasting for approximately 1 month [7]. Although the length of each anneal was minimized to mitigate the risk of fusing the spectrometer's segmented germanium crystals, one of RHESSI's detectors became unsegmented after multiple anneals [8].

COSI will be launched into an equatorial LEO (530 km, 0° inclination). In this orbit, COSI radiation damage will be dominated by trapped protons. The COSI GeDs will be enclosed by an aluminum cryostat which blocks protons < 20 MeV, and an active Bismuth Germinate (BGO) shield in a shallow well configuration, shielding the bottom and sides of the GeD array from atmospheric gamma-rays, and absorbing the majority of protons < 150 MeV which are incident from directions outside of the main field of view of the instrument. The main contribution of protons > 20 MeV will accumulate from the times during which COSI's orbit passes through the trapped proton fluence in the edge of the South Atlantic Anomaly (SAA). Two simulated space radiation environment models AP8 [9] and AP9 [10] provide estimates of the fluence originating from the SAA. Their predictions differ by two orders of magnitude, while the measured proton flux from X-ray telescope BeppoSAX (in LEO at 4° inclination) falls in between these models [11]. For our study, we adopt the conservative upper limit set by AP9 which estimates an effective proton fluence exposure of $1.1 \times 10^8 \text{ p}^+/\text{cm}^2$ over COSI's primary 2-year mission (95 % confidence level). The fluences studied in this work are based on a previous predicted orbit for COSI which would have resulted in longer paths through the SAA, higher proton fluences, and greater damage to GeDs. In 2024, COSI's orbit was confirmed at a near equatorial inclination, resulting in a lower proton fluence. As a result, the net fluence studied in this work corresponds roughly to an extended 10 year mission at COSI's confirmed orbit.

Neutron radiation induced damage to GeDs has been studied extensively [2, 12, 13, 14]. However, relatively few studies of proton irradiation on detector performance provide insight for this work. Initial study of proton radiation was carried out on planar p-type GeDs with 6 GeV protons providing fluences ranging $(0.73 - 5.7) \times 10^8 \text{ p}^+/\text{cm}^2$ [15]. The effects of irradiation included prominent low-energy tailing and an increase in FWHM which was approximately linear with fluence. The measurements from these studies concluded that protons induce damage at lower fluences than neutron irradiations. These observations, paired with a shorter timescale for annealing repair of proton damage, suggest that the damaging mechanism for protons is distinct from that of neutrons. 1.5 GeV proton irradiation of p- and n-type coaxial GeDs with net fluences on each detector within the range of $(1.18 - 1.34) \times 10^8 \text{ p}^+/\text{cm}^2$ likewise produced significant increase in FWHM and tailing at low energies [16]. Testing three detectors in parallel, while holding each at a different temperature during irradiation, revealed a greater

degradation in spectral resolution at higher detector temperatures.

Our objectives for this work are to characterize the effects of radiation damage on COSI’s spectral performance over the primary and extended missions, and to formulate and test an annealing procedure to repair said damage and restore COSI’s spectral resolution to its baseline value. Through these damage and annealing procedures, we track the spectral resolution by measuring the FWHM of the spectral line from decaying isotope Cesium 137 (Cs-137), emitting gamma-rays at 0.662 MeV. We utilize numerical charge transport simulations, including a model of trapping [17] to relate the density of charge traps within the detector volume to the resulting degradation in spectral resolution, and ultimately track how trapping defects decrease with time spent annealing at high temperatures.

2. Carrier Transport and Trapping

2.1. Primary and Secondary Traps

In this study, we attempt to understand and separate the effects on spectral resolution of (i) primary damage caused by irradiation and (ii) secondary damage caused by cycling detectors to room temperature. We draw on previous studies to layout a basic model of charge carrier trapping after irradiation and cycling detectors to room temperature [17].

The high purity germanium used in COSI detectors has a crystalline lattice structure in which charge carriers can travel, freed by incoming gamma-rays or other ionizing radiation. Primary defects are formed from irradiating the germanium with high-energy particles. These particles scatter either individual atoms or a cascade of neighboring atoms out of their position in the lattice, resulting in lattice ‘vacancies’ and atomic displacements called interstitials. Vacancies can be either individual [18] or form ‘disordered regions’ in a stream of successive atomic displacements [2]. Both types of vacancies act as traps for charge carriers, preferentially for holes.

Secondary defects form as the result of interstitial motion which takes place when the detectors are cycled to room temperature. Fourches et al. (1991b) used deep-level transient spectroscopy (DLTS) to track signatures of traps, and concluded that secondary damage is caused by the migration of individual vacancies out of the primary disordered regions, potentially combining to form divacancy sites. These sites also act as hole traps. Confirmed in previous works [19, 14] and in our experience temperature cycling this

detector, secondary defects do not form when undamaged germanium is cycled to room temperature, only when primary defects are already present. The formation of secondary defects is important to understanding the potential impacts of radiation damage as previous studies observe a more significant degradation in resolution from secondary defects than primary defects [12, 14].

2.2. Trapping Parameters

On a basic level, charge trapping is determined by the density of charge traps in the material, n , and the cross Section of the traps, σ . The total trap density will be determined by an intrinsic trap density, originating from impurities introduced in the fabrication process, and the trap density induced by external damage – in this case irradiation and room temperature cycling. The trapping cross Section σ has been shown to vary by nearly two orders of magnitude for different trapping defects when measured with DLTS [13]. When a charge cloud q_0 travels a total path length l , the charge which has not been trapped at this point q depends on a combination of n and σ such that:

$$q = q_0 e^{-l/[n\sigma]^{-1}} \quad (1)$$

As derived in Boggs & Pike (2023), the total path length is the vector combination of the net drift displacement and random thermal motions around the path of travel. Given the carrier drift velocity, v_d , and random thermal velocity, v_{th} , (Figure 1), the total distance traveled over time t is given by:

$$l = (v_{th}^2 + v_d^2)^{1/2} t \quad (2)$$

We characterize trapping via the product $[n\sigma]^{-1}$, termed the ‘trapping product’ and measured in units of cm. Under this definition, no charge trapping would correspond to an infinite trapping product. The lower the trapping product, the more trapping that occurs for a given path length l . Neither n nor σ can be measured directly from our detector resolution measurements. However, using simulations of our detectors for various trapping products, we can derive an empirical relation between $[n\sigma]^{-1}$ and the resulting spectral resolution, which we discuss further in Section .

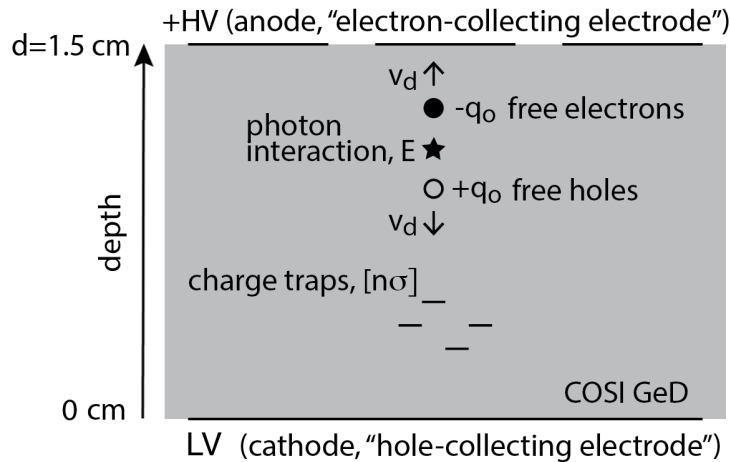


Figure 1: Charge transport in COSI GeDs

3. Methods

For this study, we used a spare p-type high purity Germanium (HPGe) cross-strip detector from the COSI-Balloon mission [20]. The detector has dimensions of 8 cm x 8 cm x 1.5 cm and 37 electrode strips of 2-mm pitch on each face. This detector depletes at 400V, and we operate it at an applied bias of +600V within an evacuated cryostat cooled by liquid nitrogen to $\sim 80\text{K}$. A gamma-ray interacting with the germanium crystal generates a cloud of electron-hole pairs from the material. Freed charges drift in the applied electric field, with the hole charge cloud collected on the LV (ground) electrode strip and the electron charge cloud on the HV (high voltage) electrode strip, as pictured in Figure 1. Each electrode is connected to readout electronics which process the signals; These are the exact readout electronics used on the COSI-Balloon payload as described in Beechert et al (2020). Events are then binned into energy spectra for analysis. To calibrate the detector and measure the spectral resolution prior to any radiation or annealing, we collected photopeak events from gamma-ray sources across a range of energies in the MeV band.

In this work, we focus on spectral measurements of the 0.662 MeV line from Cs-137. We measure the spectral resolution of the electron-collecting (AC) and hole-collecting (DC) strips separately, which enables us to distinguish between the effects of electron and hole trapping.

3.1. Radiation Damage

In order to replicate the proton fluence we might expect over COSI's mission, we used the proton synchrotron at the James M Slater MD Proton Treatment and Research Center at Loma Linda University Medical Center. We irradiated our detector in two rounds with protons with an average energy of 150 MeV incident on the HV face of the detector. During the first round, the detector received a fluence of $2.00 \times 10^8 \text{ p}^+/\text{cm}^2$. Then, after measuring the spectral resolution of the detector, we delivered another $2.95 \times 10^8 \text{ p}^+/\text{cm}^2$, resulting in a net fluence of $4.95 \times 10^8 \text{ p}^+/\text{cm}^2$. During irradiation, the detector was kept under vacuum at operating temperature ($\sim 80\text{K}$). Our measurements of the spectral resolution after each round of radiation revealed a significant broadening in photopeaks of hole-collecting strips, characteristic of increased hole trapping due to radiation damage. After completing our post-irradiation measurements, we cycled the detector to room temperature for 336 hours while keeping it under vacuum.

3.2. Annealing

To repair the primary damage from the proton fluence, in addition to the secondary damage caused by cycling the detector to room temperature after irradiation, we proceeded with seven incremental anneals to characterize the progress towards restoring the spectral resolution. These anneals are listed in Table 1.

After each annealing procedure we returned the detector to its operating temperature and collected data from a Cs-137 source, tracking the spectral resolution through the resulting FWHM of the 0.662 MeV line. Radiation damage and annealing at room temperature produced non-gaussian line profiles including low-energy tailing, spectral line shifts, and bimodal distributions. Therefore we chose to fit the Cs-137 peaks with a univariate spline interpolation in order to obtain a FWHM measurement. We also fit the preradiation datasets using this method to maintain consistent FWHM measurements.

To probe the effectiveness of annealing procedures at different temperatures, we completed anneals at 80°C and 100°C . The 5 anneals at 100°C were intended to characterize the progress of the spectral resolution back towards its preradiation value.

Table 1. Room temperature and high-temperature anneals with their temperatures and durations

Anneal #	Temperature (°C)	Time Annealing (Hours)
Room Temp	~ 20	336
1	80	24
2	80	48
3	100	24
4	100	48
5	100	96
6	100	192
7	100	192

3.3. Numerical Simulations

In parallel to our measurements characterizing the effects of radiation and annealing on the spectral performance, we used numerical simulations to model the photopeak spectrum for a range of trapping products encompassing the anticipated levels of radiation damage. Our numerical charge transport simulations, including the model for charge trapping, are described and tested in [17].

The measured FWHM of the photopeak has two components: $FWHM_d$ attributed to the trap density caused by proton damage, and $FWHM_0$ attributed to a combination of intrinsic trap density, statistical Fano noise, and noise from electronic readout. These components add in quadrature:

$$FWHM = \sqrt{FWHM_0^2 + FWHM_d^2} \quad (3)$$

For hole-collecting strips, we equated $FWHM_0$ to the measured preradiation $FWHM_h$ (~ 2.67 keV). We tabulated the FWHM of the Cs-137 photopeak produced by our numerical simulations against their respective trapping products in order to determine a relationship between the two parameters. We interpolate this relation to pair the measured FWHM produced at each stage of damage and annealing with the corresponding hole trapping prod-

Table 2. FWHM measurements for the hole-collecting electrodes after each radiation and anneal and their hole trapping products. Columns list: (i) FWHM for hole-collecting strips, (ii) FWHM where preradiation FWHM is subtracted in quadrature leaving only FWHM attributed to damage from radiation and room temperature annealing, (iii) hole trapping products calculated from numerical simulations outlined in Section 3.3.

	FWHM _{<i>h</i>} (keV)	FWHM _{<i>d,h</i>} (keV)	$[n\sigma]_h^{-1}$ (cm)
Preradiation	2.67	–	1860 ¹
Radiation 1	17.99	17.78	104
Radiation 2	50.36	50.29	41
Room Temp	~ 168.07	~ 168.04	<10
Anneal 1	38.11	30.01	49
Anneal 2	21.11	21.06	92
Anneal 3	19.28	19.09	97
Anneal 4	17.03	16.81	114
Anneal 5	7.44	6.94	295
Anneal 6	3.09	1.55	893
Anneal 7	3.13	1.63	873

¹Derived in Pike et al. (2024, in prep.)

ucts. These FWHM values and corresponding trapping products are listed in Table 2.

4. Results

4.1. Preradiation

We measured the FWHM of the Cs-137 photopeak for hole and electron-collecting strips of 2.67 keV and 4.27 keV respectively, prior to any radiation damage or annealing. The broader resolution on the electron-collecting strips is due to AC-coupling and intrinsic electron trapping [21]. The photopeak for hole-collecting strips pictured in (Figure 4).

4.2. Post Radiation

After the first round of proton irradiation, we measure a peak with a 17.99 keV FWHM for hole-collecting strips – increased by a factor of six from preradiation. After the second round of irradiation, our measured FWHM increased to 50.36 keV, over 18 times its preradiation value. In terms of fluence, this reflects an increase of roughly 8.89 keV per 10^8 p⁺/cm² after the first round of radiation and 10.15 keV per 10^8 p⁺/cm² after the second round of radiation. These measurements demonstrate a roughly linear relationship between detector resolution and net proton fluence. This trend is confirmed in Fourches (1991b) and Fourches (1991a) for p-type GeDs, and in Kandel (1999) for SPI’s n-type GeDs, all of which underwent neutron irradiation. Likewise, this is seen in in Pehl (1978) for p-type GeDs which underwent proton irradiation. We observe widened photopeaks and low-energy tailing (Figure 2) characteristic of radiation damage.

4.3. Post Room Temperature Cycling

Previous studies report detrimental effects on the spectral resolution of radiation-damaged detectors cycled to room temperature [15, 13, 22, 14]. To understand the extent of this damage, we carried out our initial anneal by bringing the detector to $\sim 20^\circ\text{C}$ for 336 hours. The photopeak we measured after this anneal, shown in Figure 3, appears nearly bimodal, making it difficult to characterize accurately with one FWHM measurement. At this point, the detector was rendered unusable as a spectrometer.

Furthermore, the line profile is unlike any of the profiles we observed after solely primary damage. As expected, a small peak appears at the expected 0.662 MeV, however, the physical origin of the more prominent peak is unclear. It is downshifted to approximately 0.520 MeV and merging with the Compton backscatter continuum we expect from Cs-137. This shift is due to extreme trapping, demonstrating that the detector had a high trap density. However, in our charge transport models simulated with high trap densities/low trapping products, we fail to observe this artifact. This suggests that the nature of the additional trapping caused by annealing at room temperature is separate from the trapping we observed from proton irradiation and that which is modeled in our numerical simulations. The distinction between these types of traps is important to maintaining the resolution of our GeDs and warrants more extensive study beyond the scope of this work.

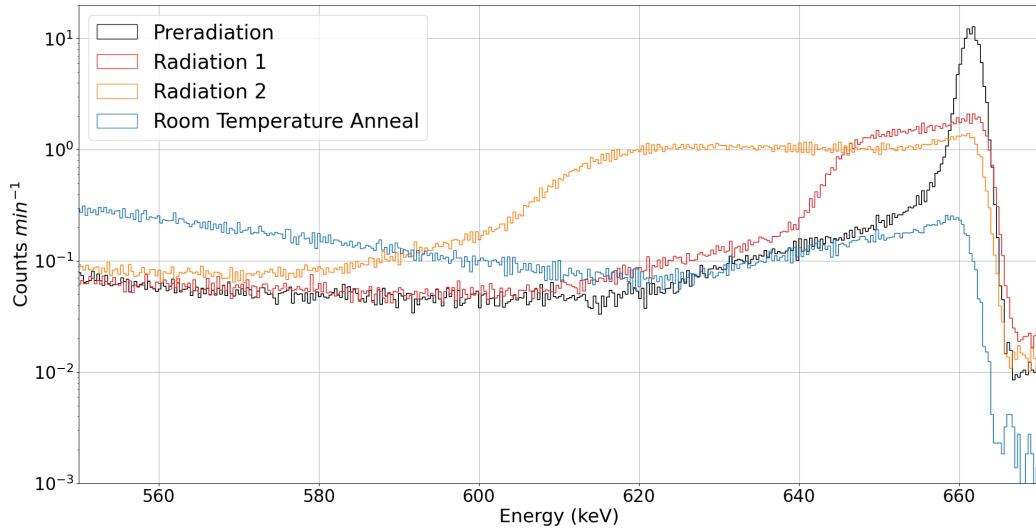


Figure 2: Counts per minute of hole-collecting strips for Cs-137 source plotted on a logarithmic scale. Counts collected: prior to radiation or annealing (black), after receiving $2.00 \times 10^8 \text{ p}^+/\text{cm}^2$ (red), after receiving a total $4.95 \times 10^8 \text{ p}^+/\text{cm}^2$ (orange), and after annealing at room temperature for 14 days (blue).

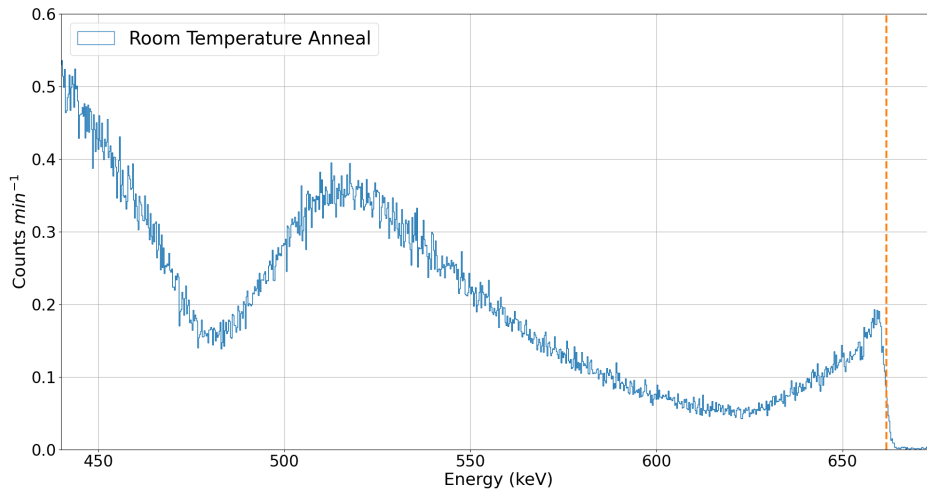


Figure 3: Counts per minute of hole-collecting strips for a Cs-137 source after annealing at room temperature for 336 hours. An orange dashed line marks 0.662 MeV, the decay energy of Cs-137.

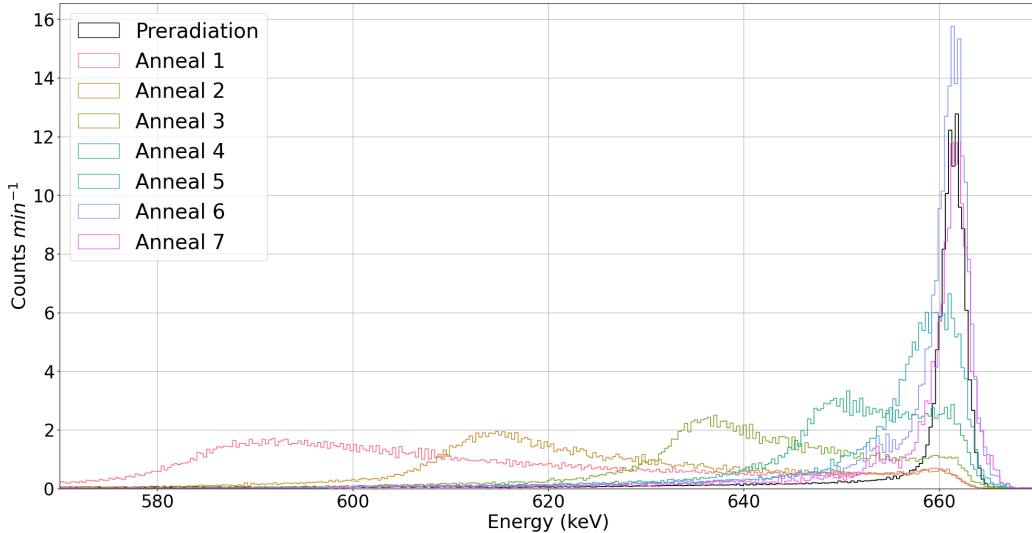


Figure 4: Counts per minute for hole-collecting strips for a Cs-137 source across incremental high-temperature anneals. Anneals and their respective FWHM measurements are listed in Table 2.

4.4. High-temperature Anneals

After the first two anneals at 80°C, summing to 72 hours, we observed FWHM_h reduced to 21.11 keV for hole-collecting strips. The photopeaks measured after each of the five 100°C anneals are plotted in Figure 4 and the repair of FWHM_d with time annealing at 100°C is marked by blue datapoints and fit to an exponential function plotted in Figure 5. The time constant for this repair is 171 ± 26 hours. This fit projects a detector spectral resolution, as measured by FWHM, will be repaired within 10% of its preradiation value in 620 ± 96 hours annealing at 100°C. When we fit this decay we assume that there is no permanent damage induced and all FWHM_d can be repaired by high-temperature anneal. Additionally we assume only the population of primary defects is present after the 80°C anneals. We justify this assumption in Section 6.1.

We use our simulation results (section 3.3) to relate Cs-137 FWHM to the trapping product (Table 2) in order to track the way in which trap density changes with time annealing at 100°C. We plot the results in Figure 6. The exponential decay fitted to this curve has a time constant of 170 ± 29 hours, a rate of repair consistent with that of FWHM_d .

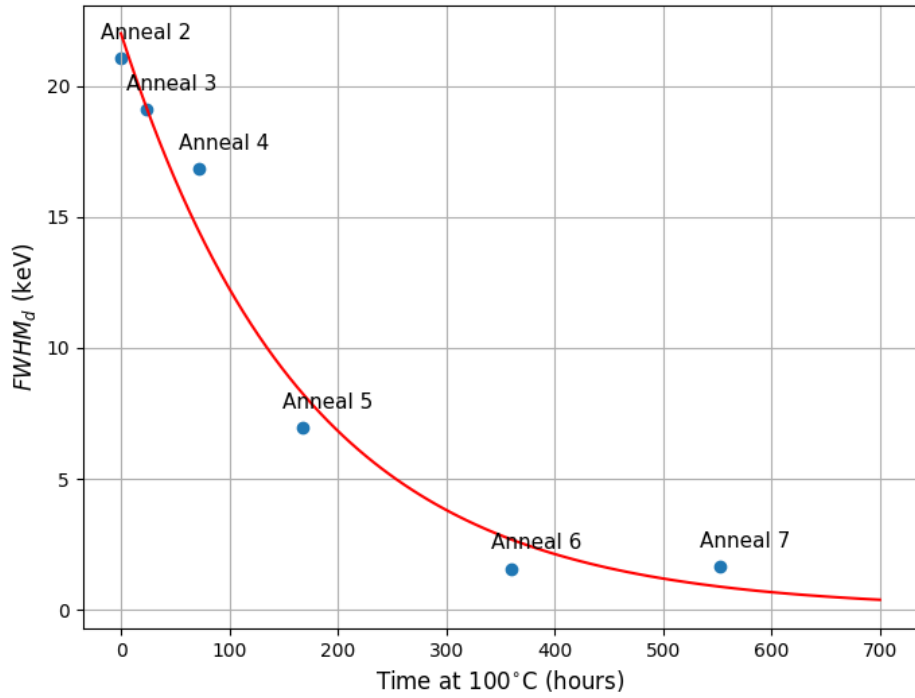


Figure 5: $FWHM_d$ (component due to radiation damage) plotted against time spent annealing at 100°C , for hole-collecting strips utilizing a Cs-137 source. An exponential decay function is fit to the datapoints and plotted in red. We find the best fit when $FWHM_{d,0} = 22.01 \pm 1.2 \text{ keV}$ and $\tau = 171 \pm 26$ hours.

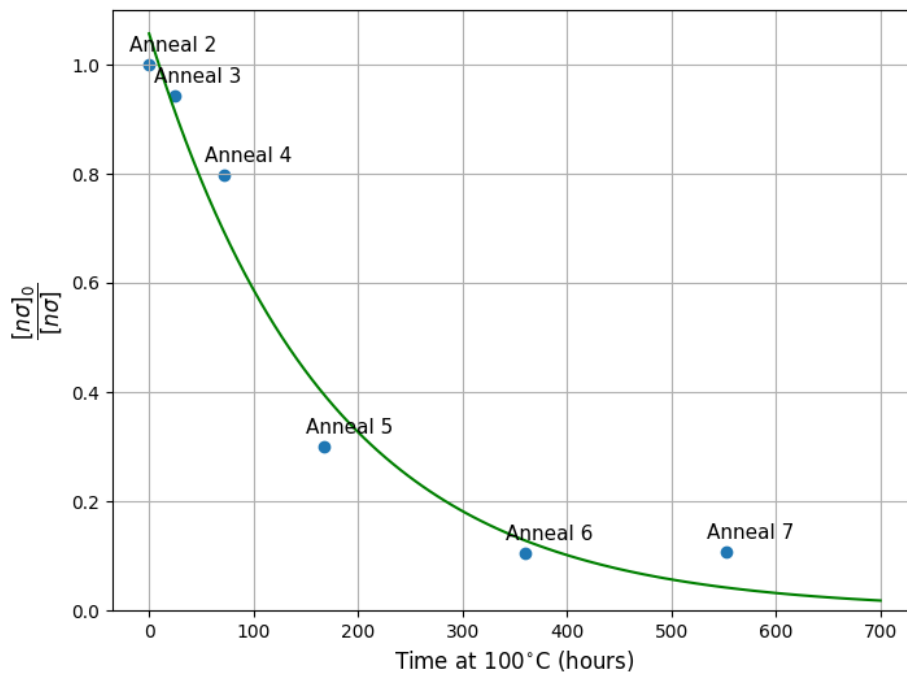


Figure 6: Decay of post-radiation trap density over time spent annealing at 100°C. The y-axis tracks the decrease in trap density (and increase in trapping product) by dividing the post-anneal 2 trapping product $[n\sigma]_0^{-1} = 93 \text{ cm}$ by the trapping product measured each successive anneal $[n\sigma]^{-1}$. An exponential decay function is fit to the data points and plotted in green. We find the best fit when $[\frac{n}{n_0}]_0 = 1.06 \pm 0.06$ and $\tau = 170 \pm 29$ hours.

5. Conclusions

We irradiated COSI GeDs with the maximum fluence expected over an extended ~ 10 year mission, and induced additional damage by cycling the detector to room temperature, increasing the FWHM by ~ 60 times its preradiation value. Through high-temperature annealing, we are able to repair the spectral resolution to within 16% of its preradiation value. This near full recovery of detector resolution demonstrates that high-temperature annealing can repair even the most heavily damaged detectors. Furthermore, our measurements enable us to characterize a repair timescale for high-energy proton damage.

The high proton fluences used in this study, along with secondary damage from room temperature cycling, significantly overestimate the damage that COSI will receive during its primary mission. Guided by the linear relationship between fluence and measured FWHM demonstrated in this study, we calculate a linear regression and obtain the projected spectral resolution at the end of COSI's primary 2-year mission. We apply the repair timescale derived in this work to estimate the anneal time needed to repair this resolution to within 10% of our current preradiation value. From these results, we anticipate that COSI spectral resolution can be repaired by annealing 100°C in 380 ± 60 hours, on the scale of two weeks. Confirming this repair time by conducting irradiation and annealing studies at lower proton fluences will be the subject of future work.

6. Discussion

6.1. Primary vs. Secondary Defect Repair

Our FWHM measurements and spectra collected after irradiation and room temperature cycling (detailed in Sections 4.2 and 4.3, respectively) indicate that there are two distinct components to induced trapping, which we have identified as the primary and secondary components. This observation is confirmed by the study of secondary defects in Fourches (1991a) and Fourches (1991b). Our goal with these first two anneals was to determine if primary damage could be annealed at lower temperatures than previously used ($\sim 100^\circ\text{C}$) on a reasonable timescale. Upon inspection, these first two anneals appear to have rapidly repaired secondary damage caused by the cycling to room temperature with little impact on primary damage.

Annealing studies completed on damaged p-type germanium have shown that the repair time of high-temperature annealing increases exponentially with decreasing temperature [18, 23]. In these studies, a 20°C temperature decrease corresponds roughly to a repair time which is five times longer [18]. To repair primary damage, previous studies report annealing times on the scale of hundreds of hours for degradations 10 -100 times larger than the target resolution, such as that which is induced in this work [22, 15]. We similarly observe repair times on the scale of hundreds of hours at 100°C as demonstrated in Section 4.4. This would imply that repair times at 80°C must be five times longer, on the scale of thousands of hours. However, in our work, we initially see a relatively rapid improvement in resolution when annealing at 80°C, on the timescale of tens of hours, but saturating at a resolution much degraded compared to the undamaged detector. This motivates us to assume that the secondary defects present prior to 80°C anneals must repair on a relatively shorter timescale ($\ll 72$ hours) at lower temperatures, while the primary defects require higher temperatures (100°C) and significantly longer anneal times.

Tracking only resolution attributed to external damage, we plot our measurements for FWHM_d for hole-collecting strips across 80°C anneals as blue data points in Figure 7 and attempt to fit decays of primary and secondary damage. We fit a double exponential function ($\text{FWHM}_d = A \cdot e^{t/\tau_1} + B \cdot e^{t/\tau_2}$) with two time constants referring to the timescales for primary and secondary annealing to the decay of FWHM_d plotted against time spent annealing. Consistent with the discussion above, we assume that the portion of FWHM_d attributed to primary defects must stay relatively constant from reaching room temperature to the end of 80°C annealing (i.e $\tau_1 \gg 72$ hours). The resulting decays of FWHM_d , along with $\text{FWHM}_{d,pri}$ and $\text{FWHM}_{d,sec}$, are plotted in Figure 7 with a time constant for the repair of secondary defects $\tau_2 = 11.15 \pm 0.09$ hours.

This indicates that secondary defects, while detrimental to spectral performance, repair at lower temperatures and significantly faster than primary defects. We conclude that 80°C annealing procedures will not repair primary defects on a reasonable timescale for an instrument in space.

6.2. Formation of Secondary Defects

We find that, for hole-collecting strips, primary defects remaining after the room temperature cycling must account for ~ 21 keV, a smaller amount of damage than we observe from the FWHM after the second round of radiation

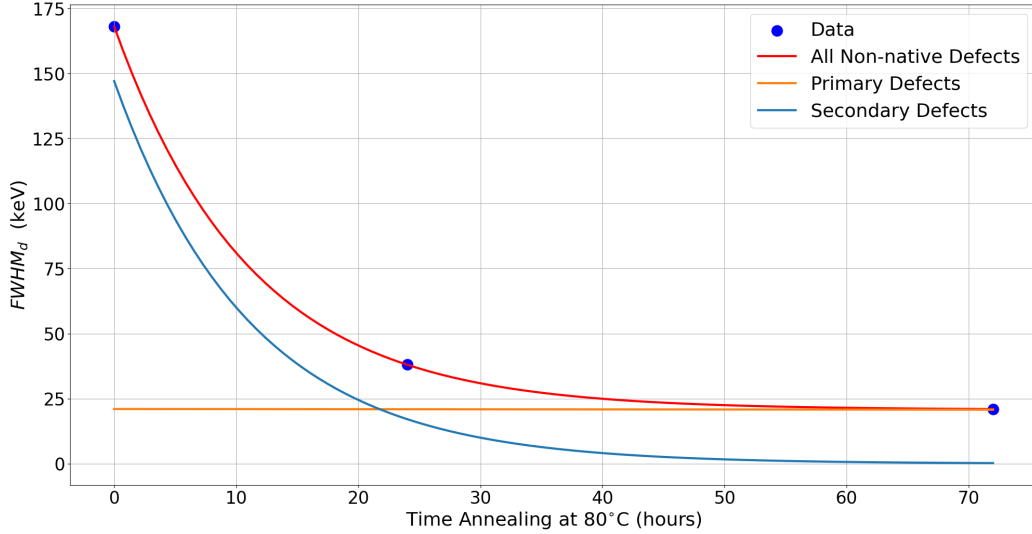


Figure 7: Anneals at 80° fitted by a double exponential function plotted in red. Decay for primary defects, assuming $\tau_1 \gg 72$ hours, is plotted in orange, while decay for secondary defects is plotted in blue.

(~ 50 keV). This suggests that a portion of the primary defects observed after radiation have been transformed into secondary defects when the detector was cycled to room temperature. This effect is observed in Fourches (1991b) which compares percentages of primary defects before and after room temperature cycling, and suggests that vacancies in disordered regions migrate out of these regions formed from primary damage and associate with each other to produce divacancies or clusters responsible for secondary damage.

Additional questions remain about the nature of traps from secondary damage. Previous literature argues that these are deep traps in order to explain their effect on resolution [12]. However, our measurements taken at separate detector depths after room temperature cycling diverge from charge trapping models outlined in [17], perhaps indicating detrapping effects. This would suggest, contrary to the conclusions of this earlier work, that secondary damage produces shallow traps which are repaired on a shorter timescale and at lower temperatures compared to primary damage, as demonstrated in Section 6.1. Answering these questions is beyond the scope of this work, but could be key to maintaining the spectral resolution of GeDs operating in the space environment.

6.3. Permanent Damage

The remaining damage-induced spectral resolution after > 550 hours of 100°C annealing may be evidence of permanent damage. We spent 192 hours annealing at 100°C between anneals 6 and 7 and observe no improvement in detector resolution. The measured FWHM for hole-collecting strips after anneals 6 and 7 remains ~ 3 keV with $\text{FWHM}_d \sim 1.5$ keV. This suggests that there is some small component of damage which our high-temperature annealing cannot eliminate. It is unclear whether this remainder is sustained from irradiation or cycling to room temperature and if it could be repaired by longer or higher temperature annealing procedures. A future study, where irradiation and high-temperature annealing procedures are repeated without cycling the detector to room temperature, could answer these questions.

7. Acknowledgements

This work was supported by the NASA Astrophysics Research and Analysis (APRA) program, grant 80NSSC22K1881. The Compton Spectrometer and Imager is a NASA Explorer project led by the University of California, Berkeley with funding from NASA under contract 80GSFC21C0059. This work was supported by the Laboratory Directed Research and Development Program of Lawrence Berkeley National Laboratory under U.S. Department of Energy Contract No. DE-AC02-05CH11231. We would like to acknowledge the staff at the James M. Slater, MD, Proton Treatment and Research Center, Loma Linda University Medical Center beamline for their assistance in this study.

References

- [1] J. Tomsick, S. Boggs, A. Zoglauer, D. H. Hartmann, M. Ajello, E. Burns, C. Fryer, C. Karwin, C. Kierans, A. Lowell, J. Malzac, J. Roberts, P. Saint-Hilaire, A. Shih, T. Siegert, C. Sleator, T. Takahashi, F. Tavecchio, E. Wulf, J. Beechert, H. Gulick, A. Joens, H. Lazar, E. Neights, J. C. Martinez Oliveros, S. Matsumoto, T. Melia, H. Yoneda, M. Amman, D. Bal, P. von Ballmoos, H. Bates, M. Böttcher, A. Bulgarelli, E. Cavazzuti, H.-K. Chang, C. Chen, C.-Y. Chu, A. Ciabattini, L. Costamante, L. Dreyer, V. Fioretti, F. Fenu, S. Gallego, G. Ghirlanda, E. Grove, C.-Y. Huang, P. Jean, N. Khatiya, J. Knödseder, M. Kraus, M. Leising, T. Lewis, J. Lommler, L. Marcotulli, I. Martinez Castellanos,

- S. Mittal, M. Negro, S. Al Nussirat, K. Nakazawa, U. Oberlack, D. Palmore, G. Panebianco, N. Parmiggiani, S. Pike, F. Rogers, H. Schutte, Y. Sheng, A. Smale, J. R. Smith, A. Trigg, T. Venters, Y. Watanabe, H. Zhang, The Compton Spectrometer and Imager, in: Proc. ICRC2023, Vol. 444, 2023, p. 745. doi:<https://doi.org/10.48550/arXiv.2308.12362>.
- [2] L. S. Darken, R. C. Trammell, T. W. Raudorf, R. H. Pehl, J. H. Elliott, Mechanism for fast neutron damage of ge(hp) detectors, Nuclear Instruments and Methods 171 (1) (1980) 49–59. doi:[https://doi.org/10.1016/0029-554X\(80\)90008-7](https://doi.org/10.1016/0029-554X(80)90008-7).
- [3] G. Vedrenne, J. P. Roques, V. Schönfelder, P. Mandrou, G. G. Lichti, A. von Kienlin, B. Cordier, S. Schanne, J. Knödseder, G. Skinner, P. Jean, F. Sanchez, P. Caraveo, B. Teegarden, P. von Ballmoos, L. Bouchet, P. Paul, J. Matteson, S. Boggs, C. Wunderer, P. Leleux, G. Weidenspointner, P. Durouchoux, R. Diehl, A. Strong, M. Cassé, M. A. Clair, Y. André, SPI: The spectrometer aboard INTEGRAL, Astronomy and Astrophysics 411 (2003) L63–L70. doi:[10.1051/0004-6361:20031482](https://doi.org/10.1051/0004-6361:20031482).
- [4] R. P. Lin, B. R. Dennis, G. J. Hurford, D. M. Smith, A. Zehnder, P. R. Harvey, D. W. Curtis, D. Pankow, P. Turin, M. Bester, A. Csillaghy, M. Lewis, N. Madden, H. F. van Beek, M. Appleby, T. Raudorf, J. McTiernan, R. Ramaty, E. Schmahl, R. Schwartz, S. Krucker, R. Abiad, T. Quinn, P. Berg, M. Hashii, R. Sterling, R. Jackson, R. Pratt, R. D. Campbell, D. Malone, D. Landis, C. P. Barrington-Leigh, S. Slassi-Sennou, C. Cork, D. Clark, D. Amato, L. Orwig, R. Boyle, I. S. Banks, K. Shirey, A. K. Tolbert, D. Zarro, F. Snow, K. Thomsen, R. Henneck, A. Mchedlishvili, P. Ming, M. Fivian, J. Jordan, R. Wanner, J. Crubb, J. Preble, M. Matranga, A. Benz, H. Hudson, R. C. Canfield, G. D. Holman, C. Crannell, T. Kosugi, A. G. Emslie, N. Vilmer, J. C. Brown, C. Johns-Krull, M. Aschwanden, T. Metcalf, A. Conway, The Reuven Ramaty High-Energy Solar Spectroscopic Imager (RHESSI), Solar Physics 210 (1) (2002) 3–32. doi:[10.1023/A:1022428818870](https://doi.org/10.1023/A:1022428818870).
- [5] V. Lonjou, J. Roques, P. Von Ballmoos, P. Jean, J. Knödseder, G. Skinner, A. Thevenin, G. Weidenspointner, Characterization of the in-flight degradation of the integral/spi detectors, Nuclear Instruments

- and Methods in Physics Research Section A: Accelerators, Spectrometers, Detectors and Associated Equipment 554 (1) (2005) 320–330. doi:<https://doi.org/10.1016/j.nima.2005.08.092>.
- [6] R. Diehl, T. Siegert, J. Greiner, M. Krause, K. Kretschmer, M. Lang, M. Pleintinger, A. W. Strong, C. Weinberger, X. Zhang, Integral/spi γ -ray line spectroscopy: Response and background characteristics, *Astronomy and Astrophysics* 611 (2018) A12. doi:[10.1051/0004-6361/201731815](https://doi.org/10.1051/0004-6361/201731815).
- [7] B. Dennis, A. Y. Shih, G. J. Hurford, P. Saint-Hilaire, Ramaty High Energy Solar Spectroscopic Imager (RHESSI), Springer Nature Singapore, 2022, pp. 1–26. doi:<https://doi.org/10.1117/12.3016765>.
- [8] A. Inglis, A. Shih, The performance of RHESSI’s germanium detectors over a 16-year science mission, in: J.-W. A. den Herder, S. Nikzad, K. Nakazawa (Eds.), *Space Telescopes and Instrumentation 2024: Ultraviolet to Gamma Ray*, Vol. 13093, International Society for Optics and Photonics, SPIE, 2024, p. 130931F. doi:[10.1117/12.3016765](https://doi.org/10.1117/12.3016765). URL <https://doi.org/10.1117/12.3016765>
- [9] D. M. Sawyer, J. I. Vette, Ap-8 trapped proton environment for solar maximum and solar minimum. [AP8MAX and AP8MIN] (12 1976).
- [10] G. P. Ginet, T. O’Brien, S. L. Huston, W. R. Johnston, T. B. Guild, R. Friedel, C. D. Lindstrom, C. J. Roth, P. Whelan, R. A. Quinn, D. Madden, S. Morley, Y.-j. Su, Ae9, ap9 and spm: New models for specifying the trapped energetic particle and space plasma environment, *Space Science Reviews* 179 (1-4) (2013) 579–615, copyright - Springer Science+Business Media Dordrecht 2013; Document feature - ; Last updated - 2023-12-05. doi:<https://doi.org/10.1007/s11214-013-9964-y>.
- [11] J. Ripa, G. Dilillo, R. Campana, G. Galgoczi, A comparison of trapped particle models in low earth orbit, in: J.-W. A. den Herder, K. Nakazawa, S. Nikzad (Eds.), *Space Telescopes and Instrumentation 2020: Ultraviolet to Gamma Ray*, SPIE, 2020. doi:[10.1117/12.2561011](https://doi.org/10.1117/12.2561011).
- [12] N. Fourches, G. Walter, J. C. Bourgoin, Neutron-induced defects in high-purity germanium 4 (69) (2 1991b). doi:[10.1063/1.348728](https://doi.org/10.1063/1.348728).

- [13] N. Fourches, A. Huck, G. Walter, The role of secondary defects in the loss of energy resolution of fast-neutron-irradiated hpge gamma-ray detectors, *IEEE Transactions on Nuclear Science* 38 (6) (1991) 1728–1735. doi:10.1109/23.124169.
- [14] B. Kandel, V. Borrel, F. Albernhe, P. Frabel, B. Cordier, G. Tauzin, S. Crespin, R. Coszach, J. Denis, P. Leleux, Influence of temperature on the behaviour of integral n-type hpge detectors irradiated with fast neutrons, *Nuclear Instruments and Methods in Physics Research Section A: Accelerators, Spectrometers, Detectors and Associated Equipment* 430 (2) (1999) 363–372. doi:https://doi.org/10.1016/S0168-9002(99)00219-3.
- [15] R. H. Pehl, L. S. Varnell, A. E. Metzger, High-energy proton radiation damage of high-purity germanium detectors, *IEEE Transactions on Nuclear Science* 25 (1) (1978) 409–417. doi:10.1109/TNS.1978.4329341.
- [16] M. Koenen, J. Bruckner, M. Korfer, I. Taylor, H. Wankel, Radiation damage in large-volume n- and p-type high-purity germanium detectors irradiated by 1.5 gev protons, in: *Proceedings of 1994 IEEE Nuclear Science Symposium - NSS'94, Vol. 1, 1994*, pp. 201–205 vol.1. doi:10.1109/NSSMIC.1994.474427.
- [17] S. E. Boggs, S. N. Pike, Numerical simulations of charge trapping in germanium strip detectors (2023). arXiv:2310.01312, doi:https://doi.org/10.48550/arXiv.2310.01312.
- [18] W. L. Brown, R. C. Fletcher, K. A. Wright, Annealing of bombardment damage in germanium: Experimental, *Phys. Rev.* 92 (1953) 591–596. doi:10.1103/PhysRev.92.591.
- [19] H. Thomas, J. Eberth, F. Becker, T. Burkardt, S. Freund, U. Hermkens, T. Mylaeus, S. Skoda, W. Teichert, A. v.d Werth, P. von Brentano, M. Berst, D. Gutknecht, R. Henck, Neutron induced radiation damage of a n-type ge detector influence of the operating temperature, *Nuclear Instruments and Methods in Physics Research Section A: Accelerators, Spectrometers, Detectors and Associated Equipment* 332 (1) (1993) 215–219. doi:https://doi.org/10.1016/0168-9002(93)90761-6.

- [20] J. Beechert, H. Lazar, S. E. Boggs, T. J. Brandt, Y.-C. Chang, C.-Y. Chu, H. Gulick, C. Kierans, A. Lowell, N. Pellegrini, J. M. Roberts, T. Siegert, C. Sleator, J. A. Tomsick, A. Zoglauer, Calibrations of the Compton Spectrometer and Imager, *Nuclear Instruments and Methods in Physics Research A* 1031 (2022) 166510. [arXiv:2203.00695](https://arxiv.org/abs/2203.00695), doi:10.1016/j.nima.2022.166510.
- [21] S. N. Pike, S. E. Boggs, J. Beechert, J. Roberts, A. Y. Shih, J. A. Tomsick, A. Zoglauer, Characterizing and correcting electron and hole trapping in germanium cross-strip detectors, *Nuclear Instruments and Methods in Physics Research Section A: Accelerators, Spectrometers, Detectors and Associated Equipment* 1056 (2023) 168562. doi:<https://doi.org/10.1016/j.nima.2023.168562>.
- [22] P. N. Peplowski, M. Burks, J. O. Goldsten, S. Fix, L. E. Heffern, D. J. Lawrence, Z. W. Yokley, Radiation damage and annealing of three coaxial n-type germanium detectors: Preparation for spaceflight missions to asteroid 16 psyche and mars' moon phobos, *Nuclear Instruments and Methods in Physics Research Section A: Accelerators, Spectrometers, Detectors and Associated Equipment* 942 (2019) 162409. doi:<https://doi.org/10.1016/j.nima.2019.162409>.
- [23] T. R. Waite, Diffusion-limited annealing of radiation damage in germanium, *Phys. Rev.* 107 (1957) 471–478. doi:10.1103/PhysRev.107.471.